Comparative Performance of Molecular Sieve- and Resin-Coated Ceramic Honeycomb Beds for Carbon Dioxide Adsorption

Shi-Cheng Huang[1], Shun Gao[2], and Tsair-Wang Chung[1,*]

[1]Department of Chemical Engineering, College of Engineering, Chung Yuan Christian University, Taoyuan City, Taiwan
[2]Department of Forestry, Sichuan Agricultural University, Chengdu, Sichuan, China
Email: tinachencycu@gmail.com (S.C.H.); Shun12202@yahoo.com (S.G.); twchungcycu@gmail.com (T.W.C.)
*Corresponding author

Manuscript received December 18, 2025; accepted January 21, 2026; published February 28, 2026

***Abstract*—This study employed ceramic honeycomb tubes coated with 13X molecular sieve and purolite A110 resin as adsorbents to compare their gas adsorption performance. The effects of gas flow rate, inlet concentration, bed height, and gas composition were systematically investigated to identify the influence of operating conditions for each adsorbent. When adsorption efficiency declined below a critical threshold, breakthrough curve analysis was used to determine the optimal replacement time of the adsorbent, providing practical guidance for engineering applications. Multi-component dynamic adsorption experiments revealed competitive adsorption among gases. When carbon monoxide, carbon dioxide, and hydrogen coexisted, both 13X and A110 selectively adsorbed carbon dioxide, demonstrating their preferential affinity toward CO_2. Based on equilibrium uptake values, 13X achieved an adsorption capacity of 74.63 mg/g, while A110 reached 68.57 mg/g, indicating a higher selectivity ratio for 13X. Equilibrium adsorption experiments further showed that A110 exhibited greater adsorption capacity at low CO_2 partial pressures (low concentrations). However, as the partial pressure increased, A110's adsorption capacity plateaued, while that of 13X continued to rise. This indicates that A110 is more effective under low CO_2 concentrations, whereas 13X performs better at higher concentrations. The observed behavior is attributed to the larger pore structure and amine functional groups of A110, which enhance CO_2 binding under dilute conditions, whereas the microporous framework and high specific surface area of 13X, confirmed by Brunauer Emmett Teller (BET) analysis, contribute to its superior performance at elevated concentrations.**

***Keywords*—adsorption, selectivity, carbon dioxide, molecular sieve 13X, resin A110, honeycomb bed**

I. Introduction

The increasing emissions of carbon dioxide are the primary driver of global climate change, posing a serious threat to the health and stability of Earth's ecosystems. Consequently, extensive research has been conducted on CO_2 capture, with most studies focusing on flue gas from industrial emissions. However, relatively fewer investigations have examined the selective adsorption of syngas generated from biomass gasification processes.

During gasification, carbonaceous materials or biomass undergo drying, pyrolysis, and gasification reactions, producing biochar, tar, pyroligneous acid, and gaseous syngas [1]. Syngas consists of CO, CO_2, H_2, and CH_4, which can be directly combusted for power generation or catalytically converted into hydrocarbons and methanol, making it an essential feedstock for the petrochemical and energy industries. The most common industrial method of methanol production relies on syngas [2], synthesized via Cu–Zn-based catalysts. However, this process requires high pressure, leading to excessive energy consumption.

Both CO_2 and CO can be converted into methanol [3–4]. In the CO_2-based pathway, methanol formation is accompanied by CO and H_2O as byproducts. Therefore, by removing CO_2 and increasing the H_2/CO ratio, the methanol yield can be significantly enhanced.

Methanol is liquid at ambient temperature and pressure and, compared with hydrogen, offers advantages in storage and transport [5]. In addition to serving as a fuel, methanol can be transformed into a variety of high-value products via catalytic conversion, with applications in solvents, pharmaceuticals, and textiles. The conventional industrial methanol synthesis proceeds as follows [6]:

$$CO_2+3H_2\rightarrow CH_3OH+H_2O \quad \Delta H = -49.5 \text{ kJ/mol}$$

$$\Delta G = 3.84 \text{ kJ/mol}$$

$$CO_2 + H_2\rightarrow CO + H_2O \quad \Delta H = 41.2 \text{ kJ/mol} \quad \Delta G = 28.6 \text{ kJ/mol}$$

For comparison, the CO-based pathway is:

$$CO+2H_2\rightarrow CH_3OH \quad \Delta H = -90.5 \text{ kJ/mol} \quad \Delta G = -25.1 \text{ kJ/mol}$$

Since the Gibbs free energy change (ΔG) for the above reaction is negative, the CO-based pathway proceeds more spontaneously, achieving higher conversion and selectivity.

Adsorption is widely recognized as a promising CO_2 capture technology because it can be retrofitted to existing power plants, operated under diverse conditions, and provides relatively high capacity, selectivity, and low regeneration energy requirements. When adsorbents are derived from waste materials, the sustainability of the process can be further enhanced. Importantly, adsorption is particularly suitable for direct air capture of CO_2 [7]. Current research efforts focus on developing advanced adsorbents with improved CO_2 uptake, selectivity, and impurity tolerance. Common adsorbents include carbonaceous materials, activated alumina, silica gel, molecular sieves, and resins.

Zeolite molecular sieves are crystalline microporous aluminosilicates composed of interconnected tetrahedral units of SiO_4 and AlO_4. Due to the trivalent nature of Al, the AlO_4 tetrahedron carries a negative charge, which is balanced by cations such as alkali, alkaline earth, rare earth metals, ammonium, or protons (e.g., Na^+, K^+, Ca^{2+}, Li^+) [8]. The general structural formula is:

$$M_{x/n}[(AlO_2)_x (SiO_2)_y] \cdot wH_2O$$

where n is the cation valence. Because two AlO_4 tetrahedra cannot be directly connected, $x \leq y$, meaning the Si/Al ratio

must be ≥1. Depending on structure, the Si/Al ratio typically ranges from 1–5. The specific pore sizes and high surface area of zeolites make them attractive for applications in molecular sieving, ion exchange, adsorption, catalysis, and detergents [9, 10].

Zeolite type strongly influences adsorption capacity, with A-, X-, and Y-type zeolites being the most widely used synthetic commercial variants. A-type zeolite consists of sodalite cages linked into a three-dimensional isotropic pore system, with a Si/Al ratio of ~1.0. X- and Y-type zeolites share the same framework, but differ in Si/Al ratio (1–1.5 for X, 1.5–3.0 for Y) and cation content, affecting polarity and adsorption selectivity [11].

Zeolites are typically synthesized hydrothermally from sodium aluminosilicate gels, but using chemical-grade Si and Al precursors is costly. Therefore, cost-effective synthesis approaches employ natural clays such as kaolinite, fly ash, waste ceramics, illite, bentonite, and montmorillonite [9]. Zhao *et al.* [12] synthesized 13X zeolite from kaolinite, enhancing surface area and lowering diffusion resistance, resulting in improved CO_2 uptake. Park *et al.* [13] investigated adsorption equilibria of six gases (CO_2, CO, N_2, CH_4, Ar, H_2) on pelletized 13X zeolite, reporting CO_2 >> CO ≈ CH_4 > N_2 > Ar >> H_2. Similarly, the commercial Purolite A110 resin, like 13X, exhibits strong CO_2 selectivity. Accordingly, this study compares CO_2 adsorption performance of these two adsorbents, 13X molecular sieve and Purolite A110 resin.

The long-term performance and economic feasibility of resin-based CO_2 adsorbents are critically influenced by their thermal and chemical stability during cyclic operation. Recent studies have shown that amine-functionalized resins such as Purolite A110 maintain high CO_2 capacity over dozens of adsorption-desorption cycles under moderate regeneration conditions, with minimal capacity loss when operated below 100 °C [14]. However, exposure to oxygen, water vapor, or acid gases can accelerate oxidative or hydrolytic degradation of the amine sites, leading to gradual decline in working capacity and increased regeneration energy demand [15, 16]. The degradation pathways primarily involve formation of urea and nitrosamine species or leaching of active amines from the polymer matrix.

From an economic perspective, the lifespan of adsorbents, typically hundreds to thousands of cycles, significantly impacts the overall cost of CO_2 capture. Therefore, optimizing adsorbent regeneration conditions and developing oxidation-resistant formulations remain key to achieving cost competitiveness for large-scale or direct air capture systems.

II. Experiment

This study employed syngas components H_2, CO, and CO_2. Feed flow rates and concentrations were controlled using mass flow controllers. Dynamic adsorption experiments were conducted with stainless steel packed beds filled with the adsorbents, under varying feed flow rates, inlet concentrations, and bed heights. Concentration variations over time were measured using Gas Chromatography (GC) to characterize breakthrough behavior. Regeneration experiments were also conducted to evaluate adsorbent reusability and stability.

The adsorbents, 13X molecular sieve and purolite A110 resin, were coated on ceramic honeycomb tubes to form packed beds. Purolite A110 resin consists of macroporous polystyrene-divinylbenzene beads, commonly applied in CO_2 and aldehyde adsorption, acid removal, and decolorization. Brunauer Emmett Teller (BET) analysis indicated specific surface areas of 632.64 m²/g and 28 m²/g, with pore volumes of 0.121 cm³/g and 0.23 cm³/g for 13X and A110, respectively. Literature shows that 13X exhibits Type I and Type IV isotherms (microporous and mesoporous structures), while A110 corresponds to Type III (macroporous) [14]. The schematic of the dynamic adsorption system is shown in Fig. 1.

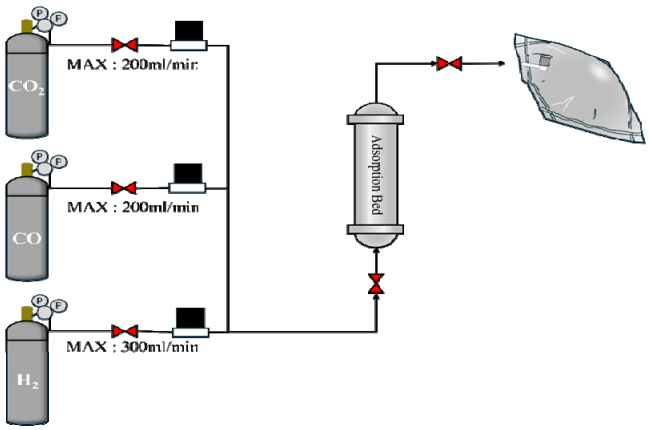

Fig. 1. Schematic diagram of the dynamic adsorption system.

The effluent gas passing through the adsorption bed was collected in sampling bags and analyzed using Gas Chromatography (GC) to determine gas composition. For analyses such as hydrogen, oxygen, nitrogen, carbon dioxide, or other inorganic compounds, a Thermal Conductivity Detector (TCD) was employed as the most suitable detector. In each analysis, 0.1 mL of gas was withdrawn from the sampling bag using a syringe and injected into the GC-TCD. A CO_2 peak was consistently observed at approximately 11.2 minutes.

A. Adsorption

To ensure complete removal of moisture and impurities from the pores of the 13X molecular sieve and purolite A110 resin, the adsorbents were regenerated in a vacuum oven for 1 h at 180 °C and 90 °C, respectively. Heating times were optimized to guarantee accurate dynamic adsorption experiments without interference from residual water vapor or impurities.

Prior to introducing the target pure or mixed gases into the adsorption bed, the feed gas was passed through the system and vented at the bottom outlet of the adsorption column for 5–10 min, allowing flow rate and concentration to stabilize. This step ensured that no residual air or contaminants within the lines affected the adsorption results. Samples were then collected every 5 min in gas bags. The collected gases were analyzed by GC-TCD to monitor peak variations of each gas component. Once no further changes in peak intensity were observed, dynamic adsorption equilibrium was considered to be reached.

The chromatographic peaks at the fixed retention times of specific compounds were recorded over time, and peak areas were converted into concentration data using calibration

curves. Breakthrough curves were subsequently plotted by correlating relative concentration (C/C_0, Y-axis) with time (X-axis). These curves were then analyzed to evaluate the effects of operating parameters, including inlet concentration, feed flow rate, and bed height, on CO_2 adsorption capacity. Furthermore, competitive adsorption among CO_2, CO, and H_2 in multicomponent systems was examined, along with adsorption selectivity and behavior under ultralow CO_2 concentrations.

B. Desorption

In industrial practice, the desorption temperature for 13X molecular sieve typically ranges from 200 °C to 300 °C at atmospheric pressure. To lower the required regeneration temperature, vacuum heating was adopted. Accordingly, 13X was regenerated at 180 °C under vacuum, while purolite A110 resin was regenerated at 90 °C.

The saturated adsorbents (13X and A110) were placed in a vacuum oven, set to 180 °C and 90 °C, respectively, for 1 h. Under these conditions, adsorbed gases within the pores and on the surface of the adsorbents were desorbed. The vacuum environment further prevented re-adsorption of CO_2 or other gases from the surrounding air. Regenerated adsorbents were then collected for reuse in subsequent adsorption experiments.

III. Results and Discussion

A. Flowrate

Since the feed flow rate governs the contact time between the feed gas and the adsorbent surface or pore structure, it is a key parameter for evaluating adsorption performance in dynamic systems. Fig. 2 presents the breakthrough curves for CO_2 adsorption at different feed flow rates (100 and 200 mL/min), with other parameters kept constant. As the flow rate increased, the breakthrough curve shifted to the left, indicating earlier breakthrough. Specifically, the breakthrough time (t_b at $C/C_0 = 0.05$) decreased from 34 min to 13.3 min. The total CO_2 uptake, calculated from the area under the breakthrough curve, was 1233.63 mg and 1273.86 mg, respectively.

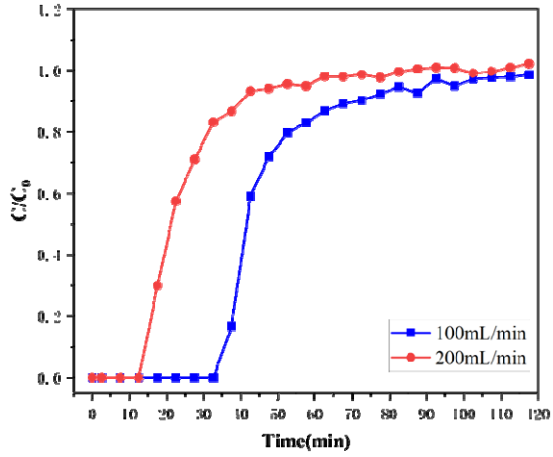

Fig. 2. Breakthrough curves of CO_2 adsorption on 13X at different feed flow rates.

B. Concentration

The initial CO_2 concentration significantly affects adsorption behavior. A higher inlet concentration enhances the concentration gradient, thereby reducing mass transfer resistance within the adsorbent and improving adsorption efficiency. Fig. 3 compares breakthrough curves at 15 vol.% and 30 vol.% CO_2. Increasing concentration shortened the breakthrough time from 34 min to 28.1 min, while the total CO_2 uptake increased from 1233.63 mg to 1818.72 mg.

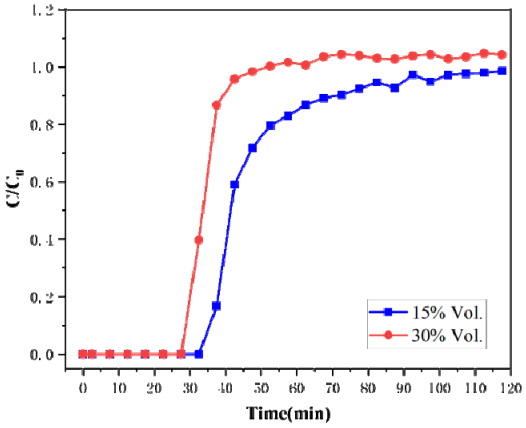

Fig. 3. Breakthrough curves of CO_2 adsorption on 13X at different inlet concentrations.

C. Bed Height

Increasing bed height extends the gas residence time and provides more adsorption sites, leading to enhanced CO_2 uptake. Fig. 4 compares breakthrough curves for bed heights of 20 cm and 40 cm. With higher beds, the breakthrough time (t_b at $C/C_0 = 0.05$) shifted from 34 min to 83 min, and the total CO_2 uptake increased from 1296 mg to 2565 mg. However, the adsorption capacity per unit mass of adsorbent remained nearly constant, indicating a linear relationship between bed height and overall uptake.

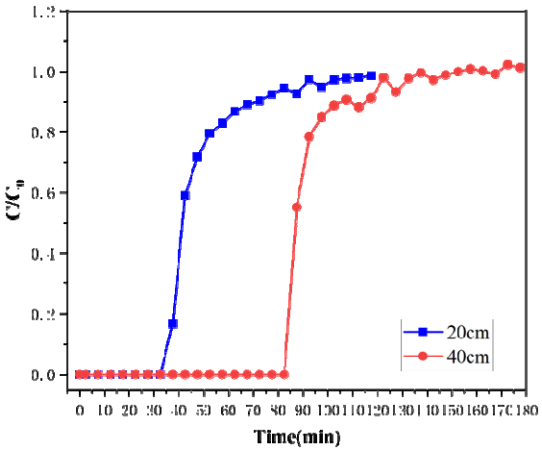

Fig. 4. Breakthrough curves of CO_2 adsorption on 13X at different bed heights.

D. Multiple Components

Gas composition in syngas depends on gasification conditions. Typical syngas contains 5–15% CO_2, 15–30% CO, and 10–20% H_2. To mimic realistic conditions, dynamic adsorption was tested with feed compositions of CO_2:CO:H_2

= 30:40:30.

Fig. 5 shows that 13X strongly favored CO_2 over CO and H_2, confirming its high CO_2 selectivity. Similarly, as shown in Fig. 6, purolite A110 resin also exhibited high selectivity for CO_2 in multicomponent mixtures. These results indicate that both adsorbents effectively discriminate CO_2 in the presence of CO and H_2.

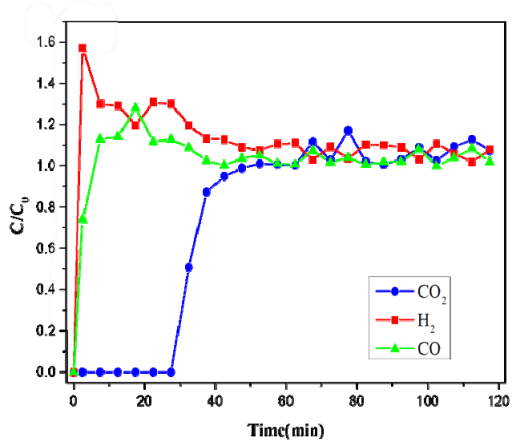

Fig. 5. Breakthrough curves of individual syngas components on 13X.

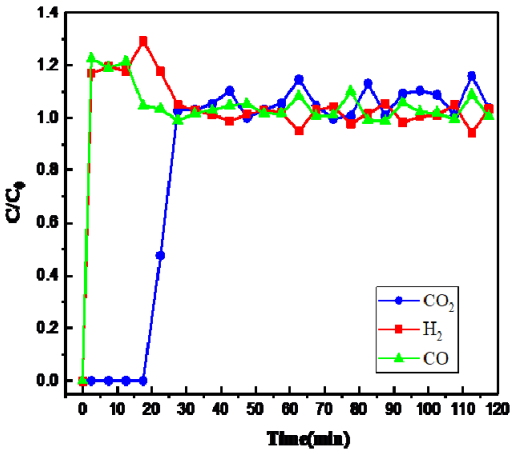

Fig. 6. Breakthrough curves of individual syngas components on purolite A110.

For single-component adsorption, the effects of parameters such as flow rate, inlet concentration, and bed height on the dynamic adsorption performance of the purolite A110 resin exhibited trends similar to those observed for the 13X molecular sieve.

E. Low Concentration

Adsorption performance at low versus high CO_2 concentrations was further investigated. For 13X, Fig. 7 shows breakthrough at 1 vol.% and 15 vol.% CO_2. The breakthrough time was longer at 1 vol.% (27.8 min) compared to 13.3 min at 15 vol.%, indicating that saturation occurred more slowly at lower concentrations.

For A110, Fig. 8 reveals an even more pronounced effect: breakthrough times were 128.2 min at 1 vol.% and 17.6 min at 15 vol.%. Thus, A110 demonstrates particularly strong performance at low concentrations, making it preferable to 13X under dilute CO_2 conditions.

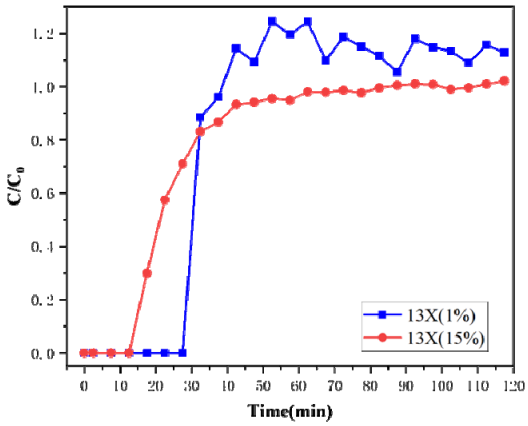

Fig. 7. Comparison of breakthrough curves for 13X at low and high CO_2 concentrations.

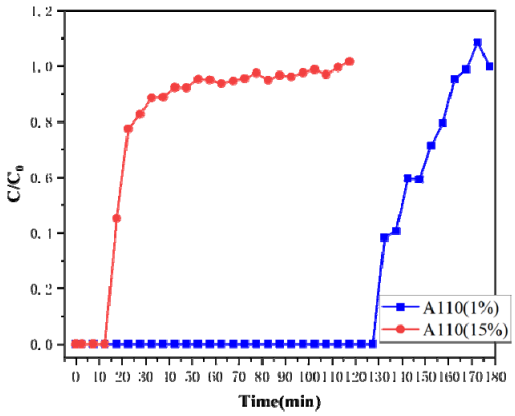

Fig. 8. Comparison of breakthrough curves for purolite A110 at low and high CO_2 concentrations.

Adsorbent regeneration was evaluated by thermal vacuum treatment (13X at 180 °C, A110 at 90 °C). After three adsorption–desorption cycles, the CO_2 uptake for 13X was 1809 mg, 1800.9 mg, and 1797.7 mg, while that for A110 was 1188 mg, 1179.9 mg, and 1739.4 mg, showing negligible degradation. These results confirm the good reusability of both materials.

F. Isotherm

Adsorption isotherms were obtained by plotting CO_2 uptake per gram of adsorbent against partial pressure (Fig. 9). At low pressures, A110 exhibited significantly higher uptake (28.83 mg/g) than 13X (4.6 mg/g). However, at higher pressures, 13X surpassed A110, with uptakes of 75.97 mg/g and 66.7 mg/g, respectively.

These findings indicate that A110 is more suitable for CO_2 capture under low-concentration conditions, while 13X is preferable at higher concentrations. The superior low-pressure performance of A110 is attributed to its macroporous structure and the presence of amine groups, which enhance CO_2 binding. Conversely, the microporous framework and high surface area of 13X favor adsorption at elevated concentrations.

At the molecular level, the adsorption mechanisms of 13X molecular sieve and purolite A110 resin differ fundamentally, mainly due to their distinct pore structures and active sites.

13X, as a zeolite with a well-defined crystalline framework, captures CO_2 primarily through physisorption, whereas purolite A110, an amine-functionalized polymeric resin, adsorbs CO_2 mainly via chemisorption. This mechanistic difference leads to the distinct adsorption behaviors observed in the experimental data: 13X exhibits higher CO_2 capacity under high partial pressure conditions, while A110 maintains good CO_2 adsorption performance even at low partial pressures.

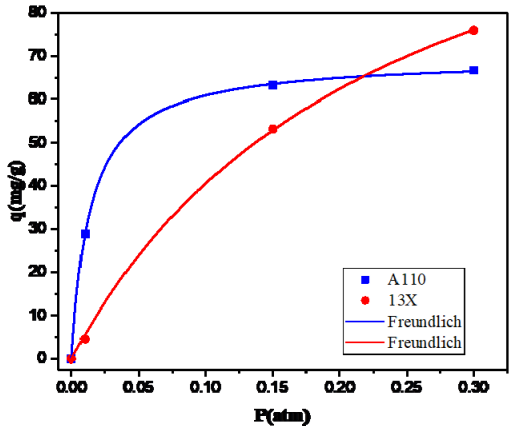

Fig. 9. Adsorption equilibrium isotherms.

IV. Conclusion

1. Effect of flow rate: In single-component dynamic adsorption, increasing the flow rate advanced the breakthrough time. The uptake remained nearly constant or a slight increase, indicating almost independence from flow rate.

2. Effect of concentration: Higher inlet CO_2 concentrations shortened breakthrough times and increased total uptake for both adsorbents, as the increased concentration gradient enhanced mass transfer driving force.

3. Effect of bed height: Doubling bed height from 20 cm to 40 cm extended breakthrough times for both adsorbents and proportionally increased total CO_2 uptake, though capacity per unit mass remained constant.

4. Multicomponent adsorption: In mixtures of CO, CO_2, and H_2, both 13X and A110 adsorbed only CO_2, confirming their strong selectivity. Uptakes were 74.63 mg/g for 13X and 68.57 mg/g for A110, demonstrating superior selectivity of 13X.

5. Equilibrium isotherms: At low CO_2 partial pressures, A110 exhibited higher uptake, while at higher pressures, 13X dominated. Thus, A110 is advantageous for dilute CO_2 capture, while 13X is optimal at elevated concentrations. This can be attributed to the macroporous structure and amine functionality of A110 versus the microporous structure and high surface area of 13X.

6. Both adsorbents demonstrated stable regeneration and reusability, confirming their potential for practical CO_2 capture applications.

Conflict of Interest

The authors declare no conflict of interest.

Author Contributions

Shi-Cheng Huang conducted the research; Shun Gao and Tsair-Wang Chung analyzed the data; Shi-Cheng Huang and Tsair-Wang Chung wrote the paper; all authors had approved the final version.

Funding

The authors acknowledge the support from Chung Yuan Christian University under the grant CYCU-WIArk-250CH.

References

[1] A. Demirbaş, "Gaseous products from biomass by pyrolysis and gasification: Effects of catalyst on hydrogen yield," *Energy Conversion and Management*, vol. 43, pp. 897–909, May 2002.

[2] M. Specht, A. Bandi, F. Baumgart, C. N. Murray, and J. Gretz, "Synthesis of methanol from biomass/CO_2 resources," *Greenhouse Gas Control Technologies Proceedings*, pp. 723–729, 1999.

[3] K. Räuchle, L. Plass, H. J. Wernicke, and M. Bertau, "Methanol for renewable energy storage and utilization," *Energy Technology*, vol. 4, pp. 193–200, January 2016.

[4] P. G. Cifre and O. Badr, "Renewable hydrogen utilisation for the production of methanol," *Energy Conversion and Management*, vol. 4, pp. 519–527, February 2007.

[5] K.-A. Adamson, and P. Pearson, "Hydrogen and methanol: A comparison of safety, economics, efficiencies and emissions," *Journal of Power Sources*, vol. 86, pp. 548–555, March 2000.

[6] N. Shamsul, S. K. Kamarudin, N. A. Rahman, and N. T. Kofli, "An overview on the production of bio-methanol as potential renewable energy," *Renewable and Sustainable Energy Reviews*, vol. 33 pp. 578–588, May 2014.

[7] M. Bui, C. S. Adjiman, A. Bardow, E. J. Anthony, A. Boston, S. Brown, and N. MacDowell, "Carbon Capture and Storage (CCS): The way forward," *Energy & Environmental Science*, vol. 11, pp. 1062–1176, May 2018.

[8] Y. Zhang, J. Sunarso, S. Liu, and R Wang, "Current status and development of membranes for CO_2/CH_4 separation: A review," *International Journal of Greenhouse Gas Control*, vol. 12, pp. 84–107, January 2013.

[9] C. Zhou, A. Alshameri, C. Yan, X. Qiu, H, Wang, and Y. Ma, "Characteristics and evaluation of synthetic 13X zeolite from Yunnan's natural halloysite," *Journal of Porous Materials*, vol. 20, pp. 587–594, August 2013.

[10] A. Kongnoo, S. Tontisirin, P. Worathanakul, and C. Phalakornkule, "Surface characteristics and CO_2 adsorption capacities of acid-activated zeolite 13X prepared from palm oil mill fly ash," *Fuel*, vol. 193, pp. 385–394, April 2017.

[11] S. Japip, H. Wang, Y. Xiao, and T. S. Chung, "Highly permeable Zeolitic Imidazolate Framework (ZIF)-71 nano-particles enhanced polyimide membranes for gas separation," *Journal of Membrane Science*, vol. 467, pp. 162–174, October 2014.

[12] Z. Zhao, X. Cui, J. Ma, and R. Li, "Adsorption of carbon dioxide on alkali-modified zeolite 13X adsorbents," *International Journal of Greenhouse Gas Control*, vol. 1, pp. 355–359, July 2007.

[13] Y. Park, Y. Ju, D. Park, and C. H. Lee, "Adsorption equilibria and kinetics of six pure gases on pelletized zeolite 13X up to 1.0 MPa: CO_2, CO, N_2, CH_4, Ar and H_2," *Chemical Engineering Journal*, vol. 292, pp. 348–365, May 2016.

[14] M.-Y. A. Low, D. Danaci, H. Azzan, R. T. Woodward, and C. Petit, "Measurement of physicochemical properties and CO_2, N_2, Ar, O_2, and H_2O unary adsorption isotherms of purolite A110 and lewatit VPOC 1065 for application in direct air capture," *J. Chem. Eng. Data*, vol. 68, pp. 3499–3511, December 2023.

[15] F. Raganati, F. Miccio, and P. Ammendola, "Adsorption of carbon dioxide for post-combustion capture: A review," *Energy Fuels*, vol. 35, pp. 12845–12868, August 2021.

[16] S. Zhao, Y. Zhang, L. Li, J. Feng, W. Qiu, Y. Ning, Z. Huang, H. Lin, "Degradation of amine-functionalized adsorbents in carbon capture and direct air capture applications: Mechanism and solutions," *Separation and Purification Technology*, vol. 354, 129586, February 2025.